Annals of Botany **133**: 521–532, 2024
https://doi.org/10.1093/aob/mcae016, available online at www.academic.oup.com/aob

ANNALS OF BOTANY
Nonprofit since 1887

Xylem-dwelling pathogen unaffected by local xylem vessel network properties in grapevines (*Vitis* spp.)

Ana Clara Fanton[1,*,†], Martin Bouda[2] and Craig Brodersen[1]

[1]School of the Environment, Yale University, New Haven, CT, USA and [2]Institute of Botany, Czech Academy of Sciences, Průhonice, Czechia[†]Current address: Ecophysiologie et Génomique Fonctionnelle de la Vigne, INRAE, Bordeaux, France
[*]For correspondence. E-mail ana.fanton@inrae.fr

Received: 11 January 2024 Editorial decision: 31 January 2024 Accepted: 7 February 2024

• **Background and aims** *Xylella fastidiosa* (*Xf*) is the xylem-dwelling bacterium associated with Pierce's disease (PD), which causes mortality in agriculturally important species, such as grapevine (*Vitis vinifera*). The development of PD symptoms in grapevines depends on the ability of *Xf* to produce cell-wall-degrading enzymes to break up intervessel pit membranes and systematically spread through the xylem vessel network. Our objective here was to investigate whether PD resistance could be mechanistically linked to xylem vessel network local connectivity.
• **Methods** We used high-resolution X-ray micro-computed tomography (microCT) imaging to identify and describe the type, area and spatial distribution of intervessel connections for six different grapevine genotypes from three genetic backgrounds, with varying resistance to PD (four PD resistant and two PD susceptible).
• **Key results** Our results suggest that PD resistance is unlikely to derive from local xylem network connectivity. The intervessel pit area (A_i) varied from 0.07 ± 0.01 mm^2 mm^{-3} in Lenoir to 0.17 ± 0.03 mm^2 mm^{-3} in Blanc do Bois, both PD resistant. Intervessel contact fraction (C_p) was not statically significant, but the two PD-susceptible genotypes, Syrah (0.056 ± 0.015) and Chardonnay (0.041 ± 0.013), were among the most highly connected vessel networks. Neither A_i nor C_p explained differences in PD resistance among the six genotypes. Bayesian re-analysis of our data shows moderate evidence against the effects of the traits analysed: A_i (BF_{01} = 4.88), mean vessel density (4.86), relay diameter (4.30), relay density (3.31) and solitary vessel proportion (3.19).
• **Conclusions** Our results show that radial and tangential xylem network connectivity is highly conserved within the six different *Vitis* genotypes we sampled. The way that *Xf* traverses the vessel network may limit the importance of local network properties to its spread and may confer greater importance on host biochemical responses.

Key words: Grapevine (*Vitis* spp.), intervessel pit area, vascular pathogens, vessel contact fraction, vessel diameter, vessel density, X-ray microcomputed tomography, *Xylella fastidiosa*, xylem vessel network.

INTRODUCTION

Vascular-wilt pathogens pose a particular threat to woody angiosperms since their colonization of the xylem provokes water transport dysfunction. Control or curative management strategies of this pathogen group are normally ineffective, and the most effective control strategy thus far is genetic resistance (Pearce, 1996; Yadeta and Thomma, 2013). Since the xylem is a heterogeneous tissue, the spatial organization for its defence should play an important role in the ability to compartmentalize and isolate the infested area. The CODIT model (compartmentalization of damage/dysfunction in trees; Shigo, 1985; Morris *et al.*, 2016, 2020) provides a generalized framework for how the xylem, through the living-cell network, can produce anatomical barriers that restrict the movement of pathogens. The model proposes that the initial barriers of defence restrict the axial movement of pathogens through the production of pathogenicity-related proteins, phytoalexins or tyloses in the vessel lumen of affected tissue. As these pathogens spread within the xylem vessel network, axial water flow decreases mostly by the production of tyloses, in species that produce it, occluding the vessels (Sun *et al.*, 2013; Pérez-Donoso *et al.*, 2016; Fanton *et al.*, 2022) in an attempt to compartmentalize the infected area (Morris *et al.*, 2016, 2020).

While bulk water transport occurs in the axial direction, anatomical configurations within the xylem network provide alternative flow pathways via radial and tangential connections between locally adjacent conduits (Tyree and Zimmermann, 2002; Brodersen *et al.*, 2013*a*; Bouda *et al.*, 2019; McElrone *et al.*, 2021; Wason *et al.*, 2021). These pathways are thought to increase the redundancy of the xylem vessel network and allow for water to be rerouted around dysfunctional sections of the xylem (Carlquist, 1988; Mrad *et al.*, 2021), where drought-induced embolism (Choat *et al.*, 2018), mechanical damage and xylem-dwelling pathogens can disrupt the flow of water. However, it is still unclear how these intervessel connections influence the systemic spread of vascular pathogens.

Additionally, more complex intervessel connections exist in some genera (e.g. *Vitis*) where vessel relays, chains of short, narrow-diameter vessel elements, link large-diameter vessels within xylem sectors delineated by rays (i.e. in the radial direction) or across rays (i.e. tangential connections) (Brodersen *et*

al., 2013*a*). Local interconduit connection number and placement could then facilitate the spread of vascular-wilt pathogens since they may rely on these pathways for tissue colonization (Tyree and Zimmermann, 2002). For example, if axial pathways become obstructed by tyloses, pathways through lateral intervessel connections may provide an alternative route. An analysis of xylem vessel network connectivity will, therefore, provide a better understanding of whether and how these different types of intervessel connections impede the spread of pathogens and, consequently, the ability to resist vascular diseases.

The xylem-limited bacterium *Xylella fastidiosa* (*Xf*; Wells *et al.*, 1987) is a conditional pathogen, developing diseases on some host plants and causing no obvious harm to plant health in others (Roper *et al.*, 2007; Landa *et al.*, 2022). *Xf* causes disease in economically important agricultural and forest species, including plants from the genera *Citrus* (citrus variegated chlorosis, CVC), *Olea* (olive quick decline syndrome, OQDS), *Quercus* (oak leaf scorch) and *Vitis* (Pierce's disease, PD). Transmitted by insects that feed on xylem sap of leaf petioles and young shoots (e.g. leafhopper sharpshooters and spittlebugs; Redak *et al.*, 2004), *Xf* is inserted directly in the vessel lumen during the feeding process (Backus *et al.*, 2015).

Xf resides and acts solely within the xylem conduits since it lacks a Type III secretion system (a typical bacterial machinery that delivers protein effectors into living parenchyma cells; Chatterjee *et al.*, 2008). Their Type IV pili-mediated motility (Meng *et al.*, 2005) enables axial movement. Lastly, *Xf* cells have a Type II secretion system, which is largely implicated in the secretion of extracellular enzymes required for the hydrolysis of different components of the pit membranes (e.g. β-1,4 endoglucanases and polygalacturonase; Roper *et al.*, 2007; Ingel *et al.*, 2019) allowing *Xf* to migrate between adjacent vessels.

The ability of *Xf* to multiply and spread is understood to be a key weakness of susceptible grapevines (Almeida and Nunney, 2015; Roper *et al.*, 2019; Landa *et al.*, 2022), as PD-susceptible genotypes have been shown to have higher bacterial cell counts and more axially distant populations from the inoculation site when compared to PD-resistant genotypes (Fry and Milholland, 1990; Krivanek and Walker, 2005; Krivanek *et al.*, 2005; Fritschi *et al.*, 2007; Baccari and Lindow, 2011; Sun *et al.*, 2013; Fanton *et al.*, 2022). Riaz *et al.* (2008) suggested that a yet unidentified anatomical or biochemical difference between the xylem of grapevine genotypes may play a role in their differential resistance to PD. Given that PD resistance has been associated with both lower bacterial cell counts and axial movement restriction within the xylem vessel network, our objective here was to investigate whether a mechanistic link can be established between the xylem vessel network connectivity and resistance to the radial or tangentially spread of *Xf*, of which would allow systematic bacterial spread.

Once *Xf* enters the xylem network, its movement will be determined by the physical obstacles it encounters, which include the intervessel connections and the pit membranes therein. Our goal in the present study was to analyse the spatial distribution and characteristics of the radial and tangential connections between xylem network conduits. Axial transport is largely a function of vessel length, where *Xf* would encounter vessel end-walls and their pit membranes that would need to be breached to proceed up- or downstream in the xylem. Fanton and Brodersen (2021) found differences in maximum vessel length between PD-resistant and PD-susceptible *Vitis* genotypes but found the pit membranes to be equally vulnerable to enzymatic degradation. Nonetheless, works report variability in the polysaccharide arrangement of *Vitis* pit membranes (Sun *et al.*, 2011, 2017) and possibilities for radial and tangential movement through the network that permit *Xf* systemic spread have yet to be explored.

The xylem's complex three-dimensional (3D) nature has restricted the characterization and quantification of interconduit connection number and placement. While recent work has established a new suite of tools for studying xylem network in 3D (Brodersen *et al.*, 2011; Lee *et al.*, 2013; Wason *et al.*, 2021), our understanding of the variability within the genus *Vitis* (e.g. between PD-susceptible and PD-resistant genotypes) is limited. Similar work in citrus and olive trees has recently led to a proposed threshold number or density of vessels, which may help to identify candidate genotypes of various hosts resistant to systemic spread of *Xf* (Walker *et al.*, 2023*a*).

We aimed to identify key anatomical traits that could support the systemic spread of the vascular-wilt bacterium *Xf*, with a specific focus on radial and tangential connections that have not been previously considered within this context. We analysed vessel network of six grapevine genotypes (four PD resistant and two PD susceptible) from three discrete genetic backgrounds (Varela *et al.*, 2001; Krivanek and Walker, 2005; Buzombo *et al.*, 2006; Krivanek *et al.*, 2006; Riaz *et al.*, 2008). We hypothesized that if the systemic spread of *Xf* is dependent on radial or tangential network connectivity, then PD-resistant genotypes would have fewer connections. While any single anatomical trait is unlikely to explain PD resistance fully, interconduit connection number and placement, which may facilitate *Xf* systemic spread, are a probable contributor to PD susceptibility and should be investigated. Here we build on a growing body of knowledge by studying xylem with micro-computed tomography (microCT) imaging to determine the spatial distribution of xylem network connections within the context of PD resistance within the genus *Vitis*.

MATERIALS AND METHODS

Plant material and sample preparation

We selected grapevines from three discrete genetic background with reported differences in PD resistance. Two PD-resistant genotypes with *Vitis arizonica* parentage were selected: (1) b43-17 *Vitis arizonica/candicans* (hereafter designated as Arizonica) and its daughter (2) hybrid 502-20, which is 88 % *V. vinifera* cv. Chardonnay (hereafter designated as Hybrid). Two commercial PD-resistant hybrids with *Vitis aestivalis* parentage were also selected, (3) Lenoir (syn. Jacques or Black Spanish) and (4) Blanc du Bois, which are popular in the American Southern wine industry where PD is problematic (Krivanek and Walker, 2005; Buzombo *et al.*, 2006). Lastly, two commercial wine grape varieties with reported PD susceptibility were selected, *Vitis vinifera* L. cv. (5) Syrah and (6) Chardonnay (Varela *et al.*, 2001). All cuttings were kindly provided by Dr Andrew Walker (Department of Viticulture and Enology, University of California Davis).

Grapevine plants were grown and maintained in a glasshouse on the Yale University campus from self-rooted cuttings in 4-L pots filled with a peat-based growing medium with perlite and vermiculite (Premier Pro-Mix BX, Premier Horticulture Inc.). Plants were fertilized with slow-release fertilizer (Scotts Miracle-Gro, Osmocote Plus Outdoor and Indoor, 15-09-12), irrigated daily, and provided with supplemental lighting [1000 µmol (photons) m^{-2} s^{-1} at the top of canopy) on a 16-h/8-h day/night cycle. Grapevines were of the same age and were trained with a primary trunk with one vertical cane, a lignified 1-year fruit-producing shoot (one growth ring). We excised the third internode, with a mean segment length of 4 ± 0.19 cm and diameter of 4.07 ± 0.61 mm and dehydrated them in a drying oven at 70 °C for 72 h (n = 4 stem segments per genotype).

3D xylem vessel network analysis

To study whether there is a relationship between xylem vessel network connectivity and PD resistance, we scanned the dry stem segments (n = 4 stem segments per genotype) at the X-ray microCT facility at the Lawrence Berkeley National Laboratory Advanced Light Source, beamline 8.3.2, in Berkeley, CA, USA. We used internode segments in this study since the large-diameter nodes increase the scanned volume beyond the field of view for the microCT instrument and extend the computational cost beyond the capabilities of our hardware and software. Stem segments were scanned at 15 keV, yielding a series of 2D projection images captured while the segment was rotated over 180°. The 2D projection images were reconstructed into a 3D data set using TomoPy (Gürsoy *et al.*, 2014). We then averaged two reconstructions (with and without phase contrast filtering) to clearly differentiate the vessel lumen from the other xylem cells. The final 3D data sets had a voxel (volumetric pixel element) size of 3.3 $µm^3$ and included ~875 ± 150 (mean ± s.d.) seamless transverse serial slices that can be viewed in any orientation (x, y and z) of the entire stem circumference. The mean scanned segment lengths were 2.9 ± 0.4 mm. While it is currently possible to measure a single longer internode segment (Brodersen *et al.*, 2011; Bouda *et al.*, 2019; Wason *et al.*, 2021), for this comparative study, we chose to study a greater number of shorter internode samples to better capture radial and tangential connections, as well as increasing our sample size to study variability between genotypes. We also measured the total xylem volume (excluding phloem, bark and pith) of each scanned segment to normalize traits between samples.

The reconstructed microCT images were processed to reconstruct the vessel network using Avizo Software 2020.2 (FEI Co., Hillsboro, OR, USA) and then analysed in a custom software package called TANAX (described in detail in Brodersen *et al.*, 2011; Lee *et al.*, 2013). First, using the 'magic wand' tool in Avizo, each vessel was selected and segmented from the surrounding xylem tissue, creating a 3D representation of the vessel lumen with x, y and z coordinates for each voxel within the lumen. Once all the xylem vessels were selected and segmented, we then created an explicit set of coordinates, known as a 'distance map' in Avizo, which was used to determine the spatial relationship between the xylem vessel network components in TANAX. Lastly, we measured vessel density (number of vessels per mm^2 of xylem area; excluding bark, phloem and pith) from 2D transverse microCT cross-sections to compare those values to the total number of vessels found in the entire 3D scanned tissue volume.

Using TANAX, vessels were classified as being connected when the distance between the vessel walls was less than 14 µm and were continuously connected in the axial dimension for at least 56 µm. These thresholds were empirically verified for *Vitis* by Brodersen *et al.* (2011) using a combination of microCT, scanning electron microscopy and light microscopy, which ensures that intervessel pitting exists between the adjacent vessels. To name these connection points, we used the glossary of terms used in wood anatomy terminology of 'intervessel pit' (Chalk *et al.*, 1964). The TANAX analysis yielded intervessel pit area (A_i, mm^2 mm^{-3}) and vessel diameter (VD, µm). From these data, we determined the contact fraction (C_p, %) which is the proportion of the vessel wall area in pitted contact with an adjacent vessel. We used two steps equations where, first, we estimate the total vessel wall area (A_v, mm^2) by summing the vessel circumferences (VD π, mm) and multiplying by scan length (L, mm): $A_v = \Sigma(\text{VD}\ \pi)\ L$, assuming cylindrical geometry. Then, C_p was calculated as $C_p = 2A_i/A_v$. We multiplied A_i by 2, since pits were placed on the wall of both vessels.

Xylem vessel relays were (hereinafter referred to as relays) spatially mapped and characterized by visually evaluating the 3D data sets using Avizo 2020.2. Once a relay was identified, we rendered its volume in 3D, determined the number of relay elements linking the two larger diameter vessel elements, and the bridged distance between these two vessel elements. Connections involving relay elements (vessel–relay and relay–relay connections) were measured by TANAX. Lastly, the spatial position of each relay was determined in relation to the pith centre using the 'point probe' tool in Avizo.

We performed a one-way ANOVA to determine whether the following xylem anatomical traits were different among the six grapevine genotypes, followed by a Tukey's honest significant difference (HSD) post hoc test: (1) number of vessels, (2) vessel density (number mm^{-3}), (3) vessel grouping, (4) intervessel pit area (A_i), (5) pit contact fraction (C_p), (6) relay density (number mm^{-3}), (7) mean relay element diameter (RD), (8) mean vessel diameter (VD) and (9) maximum vessel diameter (MVD). If data were not normalized by xylem volume, we considered the xylem volume for each stem segment as an additional predictor in the one-way ANOVA. Differences were considered significant at $P < 0.05$. These statistical analyses and graphics were prepared in RStudio (Integrated Development for R. RStudio, PBC, Boston, MA), and 3D images were generated in Avizo 2020.2.

We further performed one-way ANOVA of the same traits (1–9 above) pooling the samples into two groups: resistant and susceptible. We then subjected the ANOVA outputs to Bayesian factor (BF) re-analysis following Faulkenberry (2018) to evaluate the strength of evidence against our hypotheses. Briefly, BF_{01} is defined as the Bayes ratio of marginal likelihoods in favour of the null hypothesis (H_0) over an alternative hypothesis (H_1) given the data. Various interpretations of BF_{01} generally agree that values over ~3.16 provide at least moderate evidence for the null hypothesis (Faulkenberry, 2018; Hoekstra *et al.*, 2018; Keysers *et al.*, 2020).

Finally, we tried to detect a threshold value of vessel number and density that would predict a genotype with PD resistance.

To do this, we evaluated the likelihoods of our data given a family of logistic models that imply a threshold value within our range of observations based on Walker *et al.*'s (2023*a*) model. We evaluated models with threshold values of vessel density between 15 and 30 (at intervals of 0.01) and maximum slopes of the logistic curves between 10^{-4} and 10^{2} (at intervals of 0.01 of the exponent x in 10^{x}). For vessel number, we evaluated all integer threshold values between 200 and 450. These cutoff values span the entire range of meaningful models as they include most of our observed stems in both categories, slope values below 10^{-4} are indistinguishable from the null model (no effect), and models with slope values above 100 had log-likelihood values that could not be distinguished from negative infinity. Like Walker *et al.* (2023*a*), we only counted vessels that were open to both ends of our scans. Visual inspection confirmed that the intervals were sufficiently fine for the likelihood function to be well characterized. We compared all logistic models to a null model in which stems were assigned randomly to genotypes, which determined their resistance status (i.e. the likelihood of obtaining our data from 24 independent Bernoulli tests with $n = 1$ and $P = 1/3$, reflecting the likelihood of a susceptible genotype in our dataset). These statistical analyses were performed in MATLAB (v. R2021a 2021, MathWorks Inc., Natick, MA, USA). Mean values in the Results are given ±s.d.

RESULTS

Our analysis of the grapevine internodes yielded a mean 3D xylem volume of 25.06 ± 10 mm^3 (Table 1). Vessel density on a volumetric basis ranged from 11.4 ± 1.6 vessels mm^{-3} in Syrah to 19.2 ± 6.7 vessels mm^{-3} in B. du Bois [$F(5) = 2.3$, $P = 0.083$; Table 1]. Vessel density, measured from 2D cross-sections, ranged from 17.3 ± 3.6 vessels mm^{-2} in Syrah to 30.3 ± 11.9 vessels mm^{-2} in B. du Bois [$F(5) = 1.4$, $P = 0.247$; Table 1], which are within the same range of other *Vitis* genotypes (Schubert *et al.*, 1999; Shtein *et al.*, 2017). The relationship between the number of vessels measured in a transverse cross-section and the number of vessels in the scanned 3D volume showed little variation between measurements ($R^2 = 0.986$, $P < 0.001$; Supplementary Data Fig. S1). Vessel grouping, as defined by Carlquist (1984), was not statically significant. Across all genotypes 62 ± 8 % of the vessels were classified as solitary [$F(5) = 1.6$, $P = 0.205$; Table 2), 30 % ±6 SD as vessel pairs ($F(5) = 4.9$, $P = 0.084$; Table 2] and 8 ± 3 % as vessels multiples of three or more [$F(5) = 2.3$, $P = 0.089$; Table 2]. Values for each genotype are reported in Table 2.

We found a positive linear relationship between A_i and xylem volume, indicating that A_i distribution within the internodes is relatively uniform ($R^2 = 0.637$, $P < 0.001$; Fig. 1A). A_i was significantly different among the six genotypes, but it did not correspond to PD resistance [$F(5) = 5.5$, $P < 0.05$; Fig. 1B; Table 3]. Two PD-resistant genotypes, B. du Bois and Lenoir, had contrasting A_i measurements; B. du Bois had the largest total A_i of 0.17 ± 0.03 mm^2 mm^{-3}, ~40 % greater than Lenoir (0.07 ± 0.01 mm^2 mm^{-3}; Fig. 1B; Table 3). It is worth noting that PD-resistant daughter Hybrid and PD-susceptible mother Chardonnay had a similar A_i, 0.10 ± 0.04 and 0.10 ± 0.03 mm^2 mm^{-3}, respectively. Still, Hybrid and Chardonnay A_i values were lower than for PD-resistant mother Arizonica, 0.14 ± 0.02 mm^2 mm^{-3} (Fig. 1B; Table 3). We found no clear relationship between the contact fraction (C_p) and PD resistance among the six genotypes [$F(5) = 2.0$, $P = 0.123$; Fig. 1C; Table 3]. Nevertheless, the two PD-susceptible genotypes (Syrah and Chardonnay) had some of the highest C_p values (0.056 ± 0.01 and 0.041 ± 0.01, respectively). Likewise, differences in the total vessel wall area (A_v) were not statistically significant among the six genotypes [$F(5) = 1.1$, $P = 0.391$; Table 3].

Within the 24 analysed grapevine stems, we identified 250 relays with 851 relay elements. Relays comprised between two and nine elements connecting two or more vessels radially within a ray sector or tangentially across ray parenchyma, with a mean of 3.6 ± 1.3 elements per relay chain (Fig. 2; Table 4). Relay elements bridged distances of 36–544 µm (Fig. 3A) between two vessels either within a ray sector (Fig. 2A–D) and less frequently across rays (Fig. 2E–H). We observed a general trend in which the number of relay elements increased as the distance between the bridged vessels expanded ($R^2 = 0.339$, $P < 0.05$; Fig. 3A). However, we noted that some relay elements were not always in a 'conventional' vessel element shape (e.g. axial line) and sometimes presented a 'zigzag' shape (term defined by Tyree and Zimmermann, 2002), increasing the bridged distance in a non-proportional way (Figs 2I–L and 3A). There was a positive, linear

Table 1. *Xylem traits of the studied grapevine genotypes and their resistance level to Pierce's disease (PD). Data show means ± s.d. for xylem volume, vessel density on a volumetric basis, vessel density by xylem area, vessel diameter (VD) and maximum vessel diameter (MVD). Data were processed on Aviso software and assessed through TANAX software.*

Vitis	PD	Xylem volume (mm^3)	Density (vessel mm^{-3})	Density (vessel mm^{-2})	VD (µm)	MVD (µm)
Arizonica	Resistant	21.0 ± 6.8	15.9 ± 4.6	21.2 ± 2.9	56.0 ± 26.6 b	136.0 ± 16.0 ab
Hybrid	Resistant	29.5 ± 13.9	12.7 ± 2.6	19.5 ± 9.1	60.4 ± 24.5 a	138.5 ± 11.0 a
Lenoir	Resistant	22.7 ± 2.2	12.0 ± 3.3	23.2 ± 6.2	39.2 ± 19.4 d	99.9 ± 14.9 c
B. du Bois	Resistant	17.6 ± 5.6	19.2 ± 6.7	30.3 ± 11.9	43.7 ± 19.8 c	110.6 ± 8.8 abc
Syrah	Susceptible	33.6 ± 14.0	11.4 ± 1.6	17.3 ± 3.6	56.7 ± 25.6 b	121.8 ± 23.7 abc
Chard.	Susceptible	25.9 ± 8.4	12.3 ± 2.5	21.1 ± 3.3	43.0 ± 20.3 c	102.4 ± 13.3 bc

Within a column: only if traits were significantly different ($P < 0.05$), the same lower-case letter indicates that they are not significantly different as determined by post-hoc Tukey's HSD test.

TABLE 2. *Vessel grouping. Data show the total number ± s.d. of solitary vessels, vessel pairs, and groups of three or more vessels with their proportions. Data were processed on Aviso software and assessed through TANAX software.*

Vitis	Solitary	Pairs	3+ Groups
Arizonica	190 ± 36.9 (60 %)	102 ± 30.6 (32 %)	27 ± 8.4 (8 %)
Hybrid	245 ± 53.6 (71 %)	84 ± 41.0 (23 %)	20 ± 9.0 (6 %)
Lenoir	168 ± 57.6 (62 %)	78 ± 22.1 (29 %)	24 ± 9.7 (9 %)
B. du Bois	184 ± 28.4 (59 %)	107 ± 11.2 (34 %)	20 ± 3.3 (6 %)
Syrah	209 ± 61.6 (59 %)	128 ± 69.2 (32 %)	40 ± 25 (10 %)
Chard.	189 ± 69.5 (61 %)	93 ± 2.6 (31 %)	23 ± 8.4 (8 %)

Within a column: only if traits were significantly different ($P < 0.05$), the same lower-case letter indicates that they are not significantly different as determined by post-hoc Tukey's HSD test.

TABLE 3. *Vessel network characteristics. Data show means ± s.d. for intervessel pit area (A_i), vessel wall area (A_v) and contact fraction (C_p). Data were processed on Aviso software and assessed through TANAX software.*

Vitis	A_i (mm² mm⁻³)	A_v (mm²)	C_p
Arizonica	0.14 ± 0.02 abc	158.2 ± 68	0.036 ± 0.010
Hybrid	0.10 ± 0.04 bc	178.1 ± 87	0.032 ± 0.012
Lenoir	0.07 ± 0.01 c	99.7 ± 23	0.034 ± 0.009
B. du Bois	0.17 ± 0.03 a	139.6 ± 18	0.043 ± 0.015
Syrah	0.15 ± 0.04 ab	176.6 ± 73	0.056 ± 0.015
Chard.	0.10 ± 0.03 bc	124.6 ± 48	0.041 ± 0.013

Within a column: only if traits were significantly different ($P < 0.05$), the same lower-case letter indicates that they are not significantly different as determined by post-hoc Tukey's HSD test.

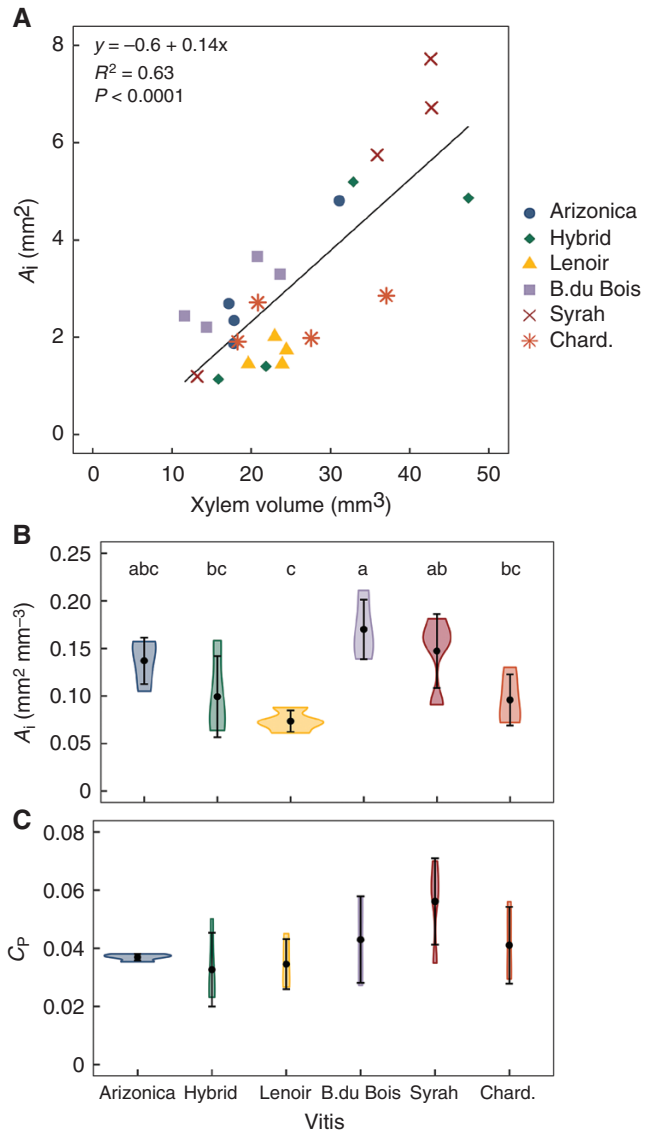

FIG. 1. (A) Relationship between intervessel pit area (A_i) and xylem volume for the six grapevine genotypes. Means of (B) A_i and (C) contact fraction (C_p). In B and C, points represent the mean ± s.d., violin shades show the data distribution. Letters indicate significant differences between genotypes based on Tukey's HSD test ($n = 4$ stems per genotype).

relationship between the number of relays and xylem volume ($R^2 = 0.328$, $P = 0.003$; Fig. 3B), suggesting that relays are added during normal xylem development for *Vitis*. For the same reasons, perhaps, the relay density (number mm^{-3}) that could facilitate *Xf* spread between two vessels otherwise classified as solitary did not differ significantly among the grapevine genotypes [$F(5) = 1.5$, $P = 0.213$; Fig. 3C; Table 4], even though mother Arizonica had a relay density over twice as high as daughter Hybrid (0.58 ± 0.2 and 0.28 ± 0.1, respectively; Fig. 3C; Table 4). Mean RD distribution was not significantly different among the six grapevine genotypes, ranging from 17.3 ± 3 µm in Lenoir to 36.5 ± 14 µm in Arizonica [$F(5) = 1.5$, $P = 0.233$; Table 1]. We also found a positive linear relationship between RD and VD means ($R^2 = 0.364$, $P < 0.05$; Fig. 3D). Despite the mean RD being smaller than the mean VD, their diameters were proportional.

In grapevine canes, vessel lateral zones (Fig. 4A, B) are associated with water transport to the leaves, tendrils and fruit clusters, while the dorsal/ventral zones (Fig. 4A, B) transport water over longer axial distances and do not generally terminate in the nodes, and typically are of a smaller diameter than vessels in the dorsal and ventral zones (Chatelet *et al.*, 2006; Brodersen *et al.*, 2011, 2013*a*). Most relays were found in the dorsal/ventral zones, with fewer relays occurring in the lateral zones (Fig. 4C–H). This distribution pattern was clearly visualized in the PD-resistant Hybrid and Lenoir (Fig. 4D, E, respectively). In both genotypes, the presence of relays in the lateral zones corresponded to 5 % and 4 % of the total number of relays, respectively. In the PD-susceptible Syrah (Fig. 4G), however, relays were found to be more homogenous in spatial distribution, where lateral zones had 20 % of relays. In the other genotypes, Arizonica, B. du Bois and Chardonnay, the lateral zones had ~14 % of relays.

The 7724 analysed vessels showed a heterogeneous VD distribution (Fig. 5A) with a mean VD of 49.7 ± 10.0 µm, ranging from 39.2 ± 19.4 µm in Lenoir to 60.4 ± 24.5 µm in Hybrid [$F(5) = 186$, $P < 0.05$; Table 1], which are within the same range of other *Vitis* genotypes (Chatelet *et al.*, 2006; Pouzoulet *et al.*, 2014; Jacobsen *et al.*, 2015). MVD was also different among the grapevine genotypes but showed no relationship to PD resistance [$F(5) = 4.9$, $P < 0.05$; Fig. 5B; Table 1]. The largest

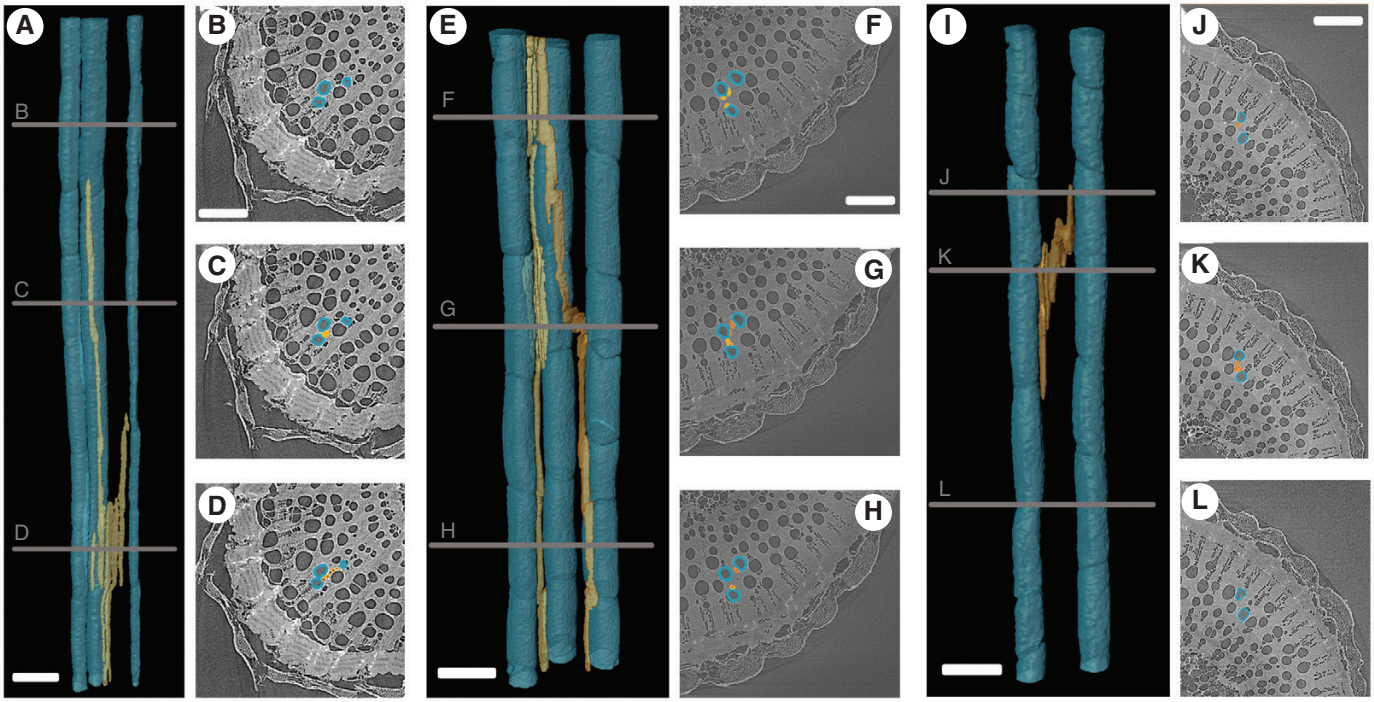

FIG. 2. (A) 3D volume renderings showing vessel relay connecting large-diameter vessels within the same radial sector. Lines B–D correspond to the respective transverse microCT images in panels B–D, with vessel outlines in blue and vessel relay outlines in yellow. (E) 3D volume renderings showing vessel relay connecting large-diameter vessels within both the same radial sector and across ray sectors (e.g. radial and tangential connections, respectively). Lines F–H correspond to the respective transverse microCT images in panels F–H, with vessel outlines in blue and vessel relay outlines in yellow. (I) 3D volume renderings showing a 'zigzag' shaped vessel relay connecting large-diameter vessels across ray sectors. Lines J–L correspond to the respective transverse microCT images in panels J–K, with vessel outlines in blue and vessel relay outlines in yellow. Bars = 250 µm.

TABLE 4. *Xylem vessel relay network characteristics. Data show means ± s.d. relay density, number of relay elements and relay element diameter (RD). Data were processed on Aviso software and assessed through TANAX software.*

Vitis genotype	Relay density (number mm^{-3})	Number of elements	RD (µm)
Arizonica	0.58 ± 0.2	3.4 ± 1.1 b	36.5 ± 27
Hybrid	0.28 ± 0.1	3.4 ± 1.0 b	33.4 ± 18
Lenoir	0.46 ± 0.3	3.8 ± 1.3 ab	17.7 ± 9
B. du Bois	0.31 ± 0.1	3.4 ± 1.0 b	18.2 ± 6
Syrah	0.47 ± 0.1	4.2 ± 1.7 a	32.7 ± 20
Chard.	0.48 ± 0.2	3.3 ± 1.2 b	20.3 ± 11

Within a column: only if traits were significantly different ($P < 0.05$), the same lower-case letter indicates that they are not significantly different as determined by post-hoc Tukey's HSD test.

mean MVD was in the Hybrid (138.5 ± 11 µm), followed by Arizonica (136.0 ± 16 µm), while the also PD-resistant Lenoir had the smallest mean MVD (99.9 ± 14.9 µm; Fig. 5B; Table 1).

Our BF analysis found moderate evidence against any effect on PD resistance by A_i ($BF_{01} = 4.88$), mean VD (4.86) and RD (4.30), relay density (3.31), or solitary vessel proportion (3.19) and only anecdotal evidence ($BF_{01} < 3.16$) for the other traits (number of vessels, vessel density, C_p and MVD). In the threshold analysis, the BF analysis was in favour of the null model (BF_{01}) exceeding 10^6 for all logistic models with slopes greater than 1/32 for vessel number models and 1/2 in vessel density (Supplementary Data Fig. S2). Further decreases of the slope parameter towards 0 led to decreases in BF_{01} as the logistic curves effectively approached the null model. No logistic models that made strong predictions (>95 %) over the range of our data yielded BF_{01} values below 100. Our observations thus provide extremely strong evidence against any threshold value of vessel number or density predicting PD resistance in grapevine and very strong evidence against the usefulness of any logistic model in these variables at all.

DISCUSSION

Our results do not support the hypothesis of a mechanistic link between PD resistance and radial and tangential xylem vessel network connectivity that would facilitate the systemic spread of *Xf* in the genotypes studied. In fact, we found various degrees of evidence against PD resistance being affected by several core conduit network properties that determine local-scale network permeability. These include increased connectivity by A_i, relay density and the proportion of solitary vessels, which characterize the spatial density of paths to traverse the network. Similarly, we found no effect on PD resistance by mean MVD

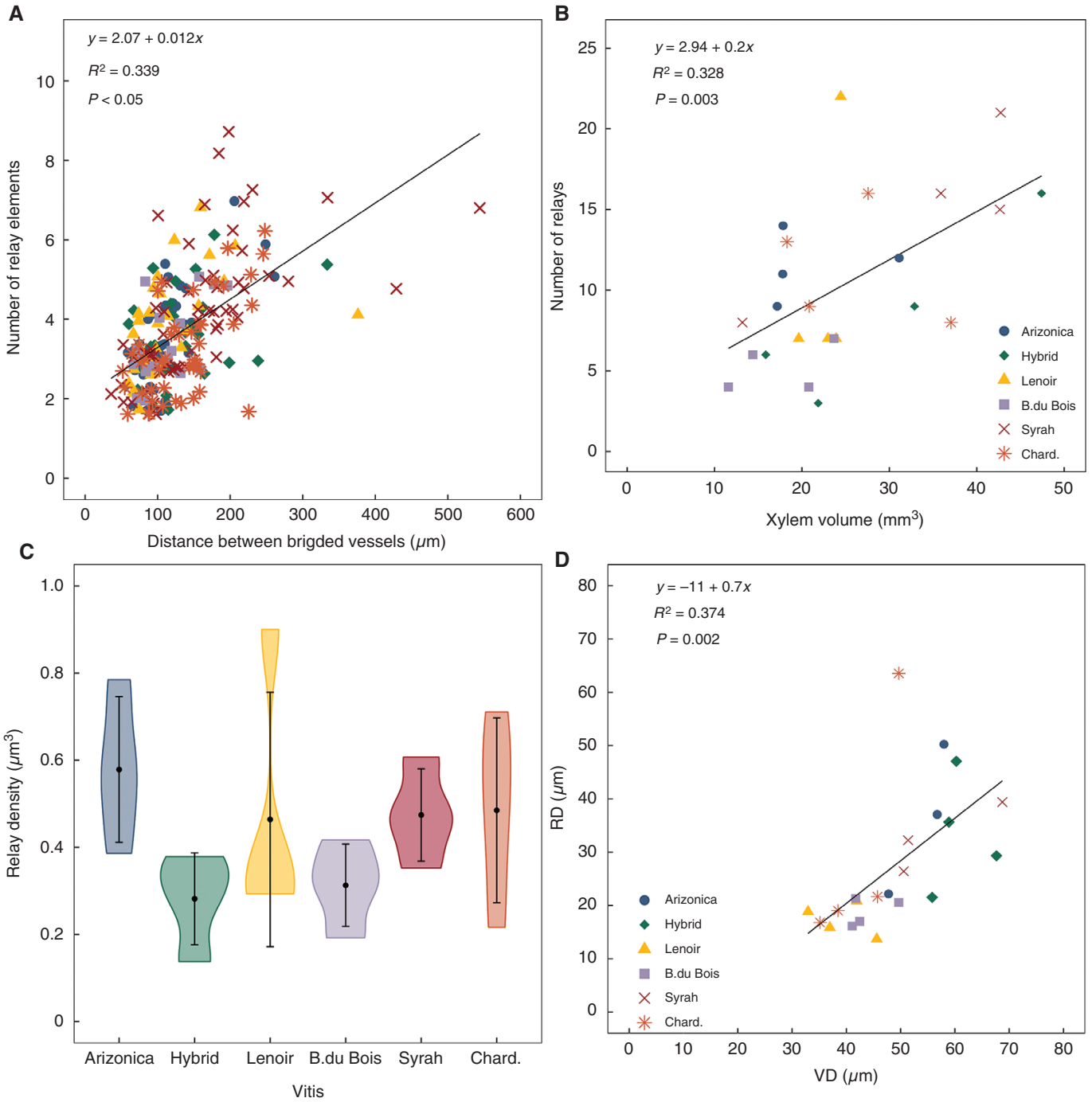

FIG. 3. (A) Relationship between the distance separating two bridged vessels and the number of vessel relay elements among the six grapevine genotypes. (B) Linear relationship of total number of relays and xylem volume for the six grapevine genotypes. (C) Relay density; points represent the mean ± s.d. and violin shades are the data distribution (n = 4 stems per genotype). (D) Linear relationship between the mean diameter of relay elements (RD) and vessels (VD) among the six grapevine genotypes (n = 851 relay elements and n = 7724 vessels).

and moderate evidence against an effect by mean VD and RD, which are the key traits determining conduit lumen permeability. Such network traits are commonly thought to facilitate embolism spread (Brodersen *et al.*, 2013*b*) and hypothesized to do the same for *Xf* (Lee *et al.*, 2013; Walker *et al.*, 2023*a*). Yet their observed effects on genotype resistance to *Xf*-related diseases are inconsistent across several commercially important species (Coletta-Filho *et al.*, 2007; Walker *et al.*, 2023*b*). Taken together, the evidence calls for a novel theory to explain why local network traits might facilitate the spread of embolism, but not *Xf* (and other xylem-dwelling pathogens).

While both embolism and pathogens rely on network permeability to spread through the xylem, differences between the mechanisms by which they overcome barriers may translate

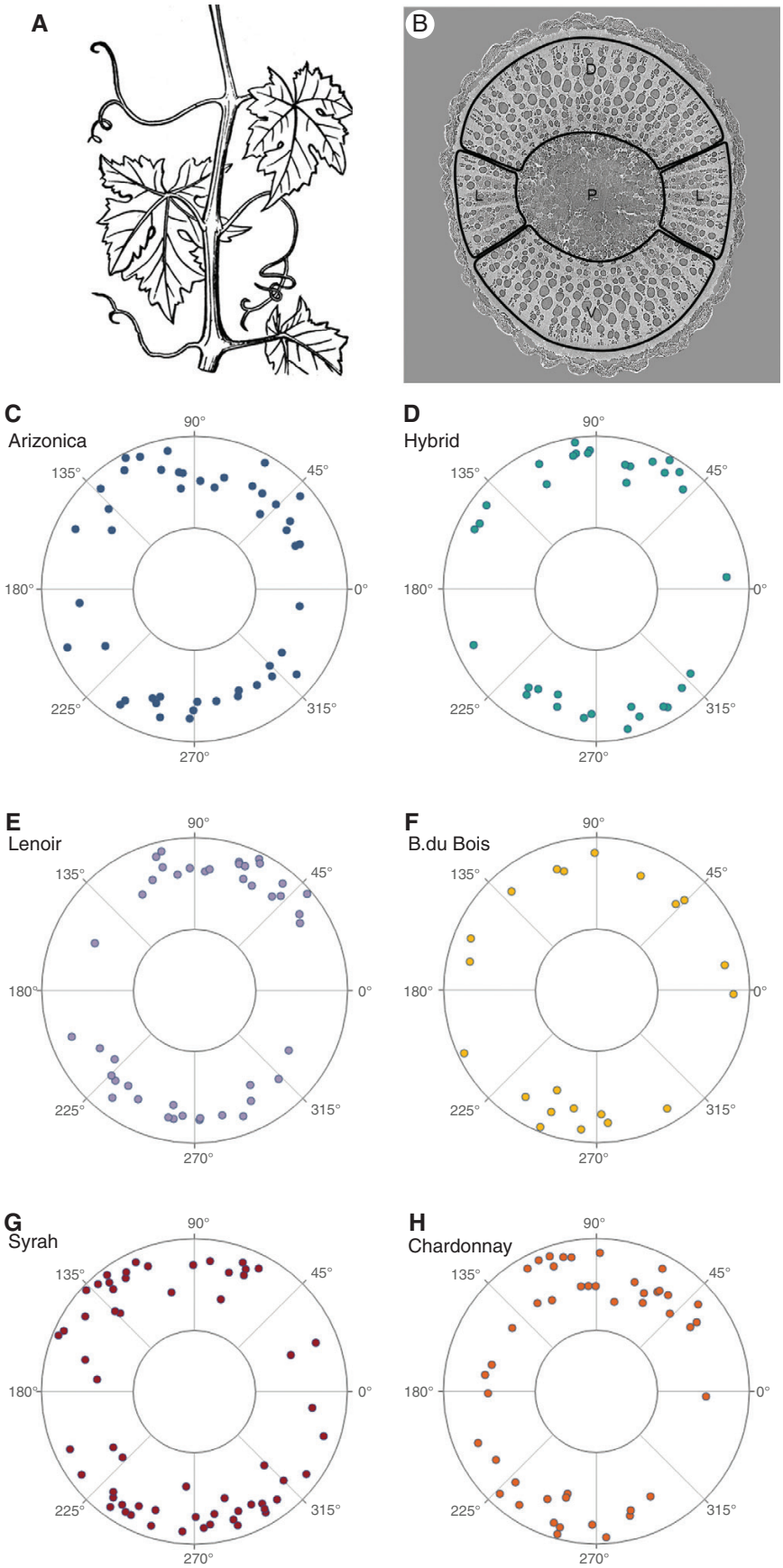

FIG. 4. (A) Botanical drawing of a grapevine cane (1-year old stem). (B) Transverse microCT image showing secondary xylem dorsal 'D', ventral 'V' and lateral 'L' zones surrounding the pith 'P'. Vessel relay locations in (C) Arizonica, (D) Hybrid, (E) Lenoir, (F) B. du Bois, (G) Syrah and (H) Chardonnay compressed into a single transverse plane. Each symbol represents the location of one vessel relay chain. The inner ring is the approximate location of the pith, and outer ring the vascular cambium. 0° and 180° are oriented to the lateral zones of the stem and 90° and 270° are oriented toward the dorsal and ventral zones of the stem, respectively.

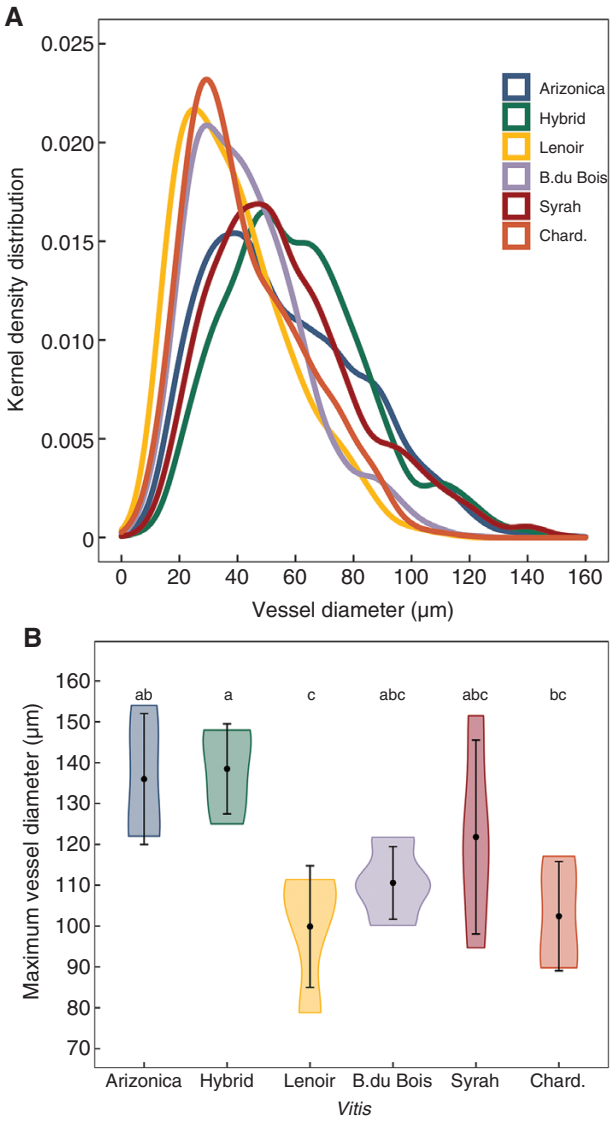

FIG. 5. (A) Vessel diameter frequency distribution for the six grapevine genotypes. Kernel density bandwidth = 0.5. (B) Mean maximum vessel diameter for the six grapevine genotypes Points represent the mean ± s.d., violin shades show the data distribution and letters indicate significant differences between genotypes based on Tukey's HSD test (n = 7724 vessels in 24 stems).

into fundamentally different ways of traversing the conduit network. Embolism spread is passive and progresses as increasing sap tension overcomes the air-seeding resistance thresholds of individual intervessel connections. Embolism occupies an entire conduit simultaneously and then continuously tests the air-seeding resistance of all connections to sap-filled conduits as the tension in the xylem increases. This can be conceived as a stochastic process, in which the distribution of air-seeding resistances is tested against the instantaneous sap tension at each connection independently, implying that spread is locally facilitated by network properties such as the number of connections each conduit has (Loepfe *et al.*, 2007; Lee *et al.*, 2013; Mrad *et al.*, 2018; Wason *et al.*, 2021; Bouda *et al.*, 2022). By contrast, *Xf* bacteria spread through the vessel network actively. Their Type IV pili-mediated motility (Meng *et al.*, 2005) enables axial movement and their Type II secretion system, which produces cell-wall-degrading enzymes to degrade the pit membranes, allows them to move from vessel to vessel. Rather than testing all available connections at once with the outcome depending on their inherent properties, membrane digestion may occur with near-certain success in susceptible genotypes depending the level of *Xf* 'effort' on a given connection. Such a process would be better represented as a choice between available connections with near-certain success at passing through the chosen ones, in which case local network properties would not be expected to affect the outcome at tissue scale. Our results indicate that the mechanistic differences between *Xf* and embolism spread at conduit scale (vessel-to-vessel) make for distinct ways of traversing the conduit network at tissue scale (systemic spread). Roughly speaking, we can think about embolism as spreading in more of a breadth-first manner while *Xf* takes more of a depth-first approach. Future modelling studies should focus on the differences among 'passive' embolism spread and active *Xf*, and other xylem-dwelling pathogens, spread.

If pathogens such as *Xf* traverse the xylem in a way that is independent of the conduit network's local structure, then vascular network intensive properties (vessel density, connectivity, etc.) are not good target traits for programmes aiming to increase resistance to their associated diseases. Indeed, our data suggest A_i, mean VD, solitary vessel proportion and vessel relay properties would make poor target traits. Moreover, our data allow us to conclusively refute the idea of a general threshold for candidate PD-resistant genotypes in terms of vessel number or density tentatively proposed by Walker *et al.* (2023*a*). Programmes for breeding resistant crop plants would probably do well to concentrate efforts elsewhere. For example, differences in pit membrane properties in *Vitis* delay *Xf* spread (Sun *et al.*, 2011, 2017; Ingel *et al.*, 2019). Consistent with the CODIT concept, global network characteristics (e.g. large-scale sectorization) may still influence susceptibility. Our study does not address these traits as they emerge at scales larger than the field of view of microCT imaging.

The broader ecological and evolutionary significance of our findings is that vascular pathogens capable of reliably breaching pit membranes and traversing the network in a directed way are not likely to exert a selection pressure on vascular network topology at local scales. This is an important open question following the recent reinterpretation of the early fossil record (Bouda *et al.*, 2022), which indicated that early evolution of vascular networks shows signs of a selection pressure by hydraulic failure. We might naively expect any noxious agent that spreads through the conduit network to effect a selection pressure reducing local connectivity. This study provides the first evidence that not all pathogens spreading through the xylem conduit network will in fact contribute to such selection.

Our results also show several proportionalities among xylem anatomical traits, which will contribute to a more accurate understanding of *Vitis* xylem network structure and how properties scale from individual conduits to the bulk tissue. First, A_i increased proportionally with xylem volume within the six genotypes (Fig. 1A), suggesting that A_i is probably conserved due to the regularity of xylem development in the genus *Vitis*. In Chardonnay, in particular, our A_i (Fig. 1B; Table 3) was consistent with another microCT analysis of a field-grown stem (0.04 mm^2 mm^{-3}; Wason *et al.*, 2021). Second, the proportion

of solitary vessels and vessels with one or more connections found here (Table 2) were also equivalent to those of Wason *et al.* (2021) (67 % and 33 %, respectively). The similarity in 3D data generated for Chardonnay internodes growing in two different environments (vineyard vs. glasshouse, California vs. Connecticut) suggests that some xylem traits are highly conserved (Tables 3 and 4). Lastly, relays were also distributed similarly among our six genotypes, which were more concentrated in the stem dorsal/ventral zones and fewer in the lateral zones (Fig. 5C–H).

The CODIT framework highlights the importance of the living-cell network that generates physical (i.e. tyloses) or biochemical (i.e. by pathogenicity-related proteins or phytoalexins) barriers to strategically restrict the movement of pathogens in the vascular system and thus reduces susceptibility to a vascular-wilt disease (Pearce, 1996; Morris *et al.*, 2016, 2020). It has been proposed that VD may impact the efficiency of the compartmentalization process as larger VD could harbour large bacterial colonies and require more tyloses (Pouzoulet *et al.*, 2014, 2017). Our results provide evidence against the effect of VD on resistance by any mechanism, including through these proposed interactions in the CODIT framework. While compartmentalization may not interact with conduit network connectivity in our data, an interesting future application of network analysis to the CODIT framework would be to consider how the 3D living-cell network is assembled (continuity of axial and ray parenchyma cells) and how this influences a plant's ability to resist *Xf* spread, for example with respect to the translocation of carbon required for the CODIT response or physical access for tylosis formation.

While *Xf* lacks a Type III secretion system, it has recently been shown to interact directly with living vascular or ray parenchyma cells in grapevine via secretions of hydrolytic enzymes that elicit production of cell wall modification enzymes by the plant to reinforce secondary cell walls (Nascimento *et al.*, 2016; Zaini *et al.*, 2018). *Vitis* is also known to produce tyloses in response to *Xf* inoculation. These immune responses may only restrict *Xf* spread at the cost of reduced xylem hydraulic conductivity, especially in PD-susceptible genotypes (Sun *et al.*, 2013; Pérez-Donoso *et al.*, 2016; Fanton *et al.*, 2022). The plants also secrete phenolic compounds, which inhibit *Xf* growth *in vitro* (Maddox *et al.*, 2010), as well as phytoalexins and pathogenesis-related proteins (Zaini *et al.*, 2018). In PD-resistant genotypes, *Xf* seems to have a more commensal relationship within these hosts as *Xf* cells do not move further than, on average, 25 cm from the inoculation point and do not develop visual symptoms (Fry and Milholland, 1990; Krivanek and Walker, 2005; Krivanek *et al.*, 2005; Fritschi *et al.*, 2007; Baccari and Lindow, 2011; Fanton *et al.*, 2022). *Xf* xylem colonization seems to be attenuated by inducing biofilm formation and attachment to the vessel walls (adhesive state; Chatterjee *et al.*, 2008; Roper *et al.*, 2019). Despite recent advances demonstrating how the xylem parenchyma cells perceive and interact with *Xf* cells, how they might avoid systemic spread (*Xf* in the planktonic, exploratory state) is still unknown and it should be explored, particularly comparing PD-resistant and PD-susceptible genotypes from different genetic backgrounds.

Despite the fact that embolism and pathogen spread follow the same pathways within the vessel network, through the intervessel connections, tracing parallels between vascular-wilt pathogens and drought has to be done carefully. PD symptoms are starkly different from water deficit symptoms, as PD is characterized by progressive necrosis of the leaf blade until it falls off (the petiole remains attached) and tyloses form in the xylem vessel lumens (Thorne *et al.*, 2006). Neither seems to happen under drought stress (Thorne *et al.*, 2006; Choat *et al.*, 2010; Gerzon *et al.*, 2015; Prats *et al.*, 2023). Active spread of the pathogen, as well as its detection and response by the parenchyma cells, appears to play a larger role in impeding *Xf* movement than the xylem vessel connectivity in the study species. Whereas some American *Vitis* species are naturally resistant to PD (coevolution pressure, Riaz *et al.*, 2020) since the centre of origin of *Xf* is the Americas (Almeida and Nunney, 2015), others, in particular the European *V. vinifera* genotypes, never had to deal with *Xf* at their centre of origins. Thus, the time to co-evolve, adapt, and resist *Xf* is probably short compared to European *V. vinifera* genotypes that had to deal with drought pressures, for example. Finally, future research efforts that compare resistant and susceptible genotypes should combine not only tools (anatomy, physiology, molecular, or biochemistry) but also genotypes from different genetic backgrounds to determine the mechanisms of PD resistance in grapevines, and other important commercially and ecologically important woody plants.

SUPPLEMENTARY DATA

Supplementary data are available at *Annals of Botany* online and consist of the following.

Figure S1: Linear relationship between the number of vessels measured in transverse sections and the number of vessels measured in the scanned volume for the six grapevine genotypes. Figure S2: Resistance to Pierce's disease plotted against number of vessels (A) and vessel density (B) for each stem ($n = 24$).

ACKNOWLEDGMENTS

We thank Dr Andy Walker for providing the grapevine plants and D. Parkinson for technical assistance at the Lawrence Berkeley National Laboratory. The Advanced Light Source is supported by the Director, Office of Science, Office of Basic Energy Sciences, of the U.S. Department of Energy under Contract No. DE-AC02-05CH11231. Lastly, Martin Bouda gratefully acknowledges funding from long-term research development project No. RVO 67985939 of the Czech Academy of Sciences.

AUTHOR CONTRIBUTIONS

A.C.F. planned the project. A.C.F. conducted the sampling and performed the Avizo software and statistical data analyses. M.B. performed the TANAX software data analysis. A.C.F. took the lead in writing the manuscript, with feedback and approval from co-authors.

LITERATURE CITED

Almeida RPP, **Nunney L. 2015**. How do plant diseases caused by *Xylella fastidiosa* emerge? *Plant Disease* **99**: 1457–1467.

Baccari C, **Lindow SE. 2011**. Assessment of the process of movement of *Xylella fastidiosa* within susceptible and resistant grape cultivars. *Phytopathology* **101**: 77–84.

Backus EA, **Shugart HJ**, **Rogers EE**, **Morgan JK**, **Shatters R. 2015**. Direct evidence of egestion and salivation of *Xylella fastidiosa* suggests sharpshooters can be 'flying syringes'. *Phytopathology* **105**: 608–620.

Bouda M, **Windt CW**, **McElrone AJ**, **Brodersen CR. 2019**. In vivo pressure gradient heterogeneity increases flow contribution of small diameter vessels in grapevine. *Nature Communications* **10**: 5645.

Bouda M, **Huggett BA**, **Prats KA**, **Wason JW**, **Wilson JP**, **Brodersen CR. 2022**. Hydraulic failure as a primary driver of xylem network evolution in early vascular plants. *Science* **378**: 642–646.

Brodersen CR, **Lee EF**, **Choat B**, ***et al***. **2011**. Automated analysis of three-dimensional xylem networks using high-resolution computed tomography. *The New Phytologist* **191**: 1168–1179.

Brodersen CR, **Choat B**, **Chatelet DS**, **Shackel KA**, **Matthews MA**, **McElrone AJ. 2013***a*. Xylem vessel relays contribute to radial connectivity in grapevine stems (*Vitis vinifera* and *V. arizonica*; Vitaceae). *American Journal of Botany* **100**: 314–321.

Brodersen CR, **McElrone AJ**, **Choat B**, **Lee EF**, **Shackel KA**, **Matthews MA. 2013***b*. In vivo visualizations of drought-induced embolism spread in *Vitis vinifera*. *Plant Physiology* **161**: 1820–1829.

Buzombo P, **Jaimes J**, **Lam V**, ***et al***. **2006**. An American hybrid vineyard in the Texas Gulf Coast: analysis within a Pierce's disease hot zone. *American Journal of Enology and Viticulture* **57**: 347–355.

Carlquist S. 1984. Vessel grouping in dicotyledon wood: significance and relationship to imperforate tracheary elements. *Aliso* **10**: 505–525.

Carlquist S. 1988. *Comparative wood anatomy.* Berlin: Springer.

Chalk L, **Huber B**, **Normand D**, **Phillips EWJ**, **Rendle BJ. 1964**. *Multilingual glossary of terms used in wood anatomy*. Verlaganstadt Buchdruckerei Konkordia: IAWA – Committee on nomenclature. International Association of Wood Anatomists, 1–46.

Chatelet DS, **Matthews MA**, **Rost TL. 2006**. Xylem structure and connectivity in grapevine (*Vitis vinifera*) shoots provides a passive mechanism for the spread of bacteria in grape plants. *Annals of Botany* **98**: 483–494.

Chatterjee S, **Almeida RPP**, **Lindow S. 2008**. Living in two worlds: the plant and insect lifestyles of *Xylella fastidiosa*. *Annual Review of Phytopathology* **46**: 243–271.

Choat B, **Drayton WM**, **Brodersen C**, ***et al***. **2010**. Measurement of vulnerability to water stress-induced cavitation in grapevine: a comparison of four techniques applied to a long-vesseled species: comparison of vulnerability curve technique in grapevine. *Plant, Cell & Environment* **33**: no–no.

Choat B, **Brodribb TJ**, **Brodersen CR**, **Duursma RA**, **López R**, **Medlyn BE. 2018**. Triggers of tree mortality under drought. *Nature* **558**: 531–539.

Coletta-Filho HD, **Pereira EO**, **Souza AA**, **Takita MA**, **Cristofani-Yale M**, **Machado MA. 2007**. Analysis of resistance to *Xylella fastidiosa* within a hybrid population of Pera sweet orange × Murcott tangor. *Plant Pathology* **56**: 661–668.

Fanton AC, **Brodersen C. 2021**. Hydraulic consequences of enzymatic breakdown of grapevine pit membranes. *Plant Physiology* **186**: 1919–1931.

Fanton AC, **Furze ME**, **Brodersen CR. 2022**. Pathogen-induced hydraulic decline limits photosynthesis and starch storage in grapevines (*Vitis* sp.). *Plant, Cell & Environment* **45**: 1829–1842.

Faulkenberry TJ. 2018. Computing Bayes factors to measure evidence from experiments: an extension of the BIC approximation. *Biometrical Letters* **55**: 31–43.

Fritschi FB, **Lin H**, **Walker MA. 2007**. *Xylella fastidiosa* population dynamics in grapevine genotypes differing in susceptibility to Pierce's disease. *American Journal of Enology and Viticulture* **58**: 326–332.

Fry SM, **Milholland RD. 1990**. Multiplication and translocation of *Xylella fastidiosa* in petioles and stems of grapevine resistant, tolerant, and susceptible to Pierce's disease. *Phytopathology* **80**: 61–65.

Gerzon E, **Biton I**, **Yaniv Y**, ***et al***. **2015**. Grapevine anatomy as a possible determinant of isohydric or anisohydric behavior. *American Journal of Enology and Viticulture* **66**: 340–347.

Gürsoy D, **De Carlo F**, **Xiao X**, **Jacobsen C. 2014**. TomoPy: a framework for the analysis of synchrotron tomographic data. *Journal of Synchrotron Radiation* **21**: 1188–1193.

Hoekstra R, **Monden R**, **Van Ravenzwaaij D**, **Wagenmakers E-J. 2018**. Bayesian reanalysis of null results reported in medicine: strong yet variable evidence for the absence of treatment effects. *PLoS One* **13**: e0195474.

Ingel B, **Jeske DR**, **Sun Q**, **Grosskopf J**, **Roper MC. 2019**. *Xylella fastidiosa* endoglucanases mediate the rate of Pierce's disease development in *Vitis vinifera* in a cultivar-dependent manner. *Molecular Plant-Microbe Interactions* **32**: 1402–1414.

Jacobsen AL, **Rodriguez-Zaccaro FD**, **Lee TF**, **Valdovinos J**, **Toschi HS**, **Martinez JA**, **Pratt RB. 2015**. Grapevine xylem development, architecture, and function. In: **Hacke UG**. ed. *Functional and ecological xylem anatomy.* Cham: Springer International Publishing.

Keysers C, **Gazzola V**, **Wagenmakers E-J. 2020**. Using Bayes factor hypothesis testing in neuroscience to establish evidence of absence. *Nature Neuroscience* **23**: 788–799.

Krivanek AF, **Walker MA. 2005**. *Vitis* resistance to Pierce's disease is characterized by differential *Xylella fastidiosa* populations in stems and leaves. *Phytopathology* **95**: 44–52.

Krivanek AF, **Stevenson JF**, **Walker MA. 2005**. Development and comparison of symptom indices for quantifying grapevine resistance to Pierce's disease. *Phytopathology* **95**: 36–43.

Krivanek AF, **Riaz S**, **Walker MA. 2006**. Identification and molecular mapping of PdR1, a primary resistance gene to Pierce's disease in *Vitis*. *TAG. Theoretical and Applied Genetics. Theoretische und angewandte Genetik* **112**: 1125–1131.

Landa BB, **Saponari M**, **Feitosa-Junior OR**, ***et al***. **2022**. *Xylella fastidiosa*'s relationships: the bacterium, the host plants, and the plant microbiome. *The New Phytologist* **234**: 1598–1605.

Lee EF, **Matthews MA**, **McElrone AJ**, **Phillips RJ**, **Shackel KA**, **Brodersen CR. 2013**. Analysis of HRCT-derived xylem network reveals reverse flow in some vessels. *Journal of Theoretical Biology* **333**: 146–155.

Loepfe L, **Martinez-Vilalta J**, **Piñol J**, **Mencuccini M. 2007**. The relevance of xylem network structure for plant hydraulic efficiency and safety. *Journal of Theoretical Biology* **247**: 788–803.

Maddox CE, **Laur LM**, **Tian L. 2010**. Antibacterial activity of phenolic compounds against the phytopathogen *Xylella fastidiosa*. *Current Microbiology* **60**: 53–58.

McElrone AJ, **Manuck CM**, **Brodersen CR**, **Patakas A**, **Pearsall KR**, **Williams LE. 2021**. Functional hydraulic sectoring in grapevines as evidenced by sap flow, dye infusion, leaf removal and micro-computed tomography. *AoB Plants* **13**: 1–12.

Meng Y, **Li Y**, **Galvani CD**, ***et al***. **2005**. Upstream migration of *Xylella fastidiosa* via pilus-driven twitching motility. *Journal of Bacteriology* **187**: 5560–5567.

Morris H, **Brodersen C**, **Schwarze FWMR**, **Jansen S. 2016**. The parenchyma of secondary xylem and its critical role in tree defense against fungal decay in relation to the CODIT model. *Frontiers in Plant Science* **7**: 1–18.

Morris H, **Hietala AM**, **Jansen S**, ***et al***. **2020**. Using the CODIT model to explain secondary metabolites of xylem in defence systems of temperate trees against decay fungi. *Annals of Botany* **125**: 701–720.

Mrad A, **Domec J-C**, **Huang C-W**, **Lens F**, **Katul G. 2018**. A network model links wood anatomy to xylem tissue hydraulic behaviour and vulnerability to cavitation. *Plant, Cell & Environment* **41**: 2718–2730.

Mrad A, **Johnson DM**, **Love DM**, **Domec J-C. 2021**. The roles of conduit redundancy and connectivity in xylem hydraulic functions. *The New Phytologist* **231**: 996–1007.

Nascimento R, **Gouran H**, **Chakraborty S**, ***et al***. **2016**. The type II secreted lipase/esterase LesA is a key virulence factor required for *Xylella fastidiosa* pathogenesis in grapevines. *Scientific Reports* **6**: 18598. doi: 10.1038/srep18598.

Pearce RB. 1996. Antimicrobial defences in the wood of living trees. *New Phytologist* **132**: 203–233.

Pérez-Donoso AG, **Lenhof JJ**, **Pinney K**, **Labavitch JM. 2016**. Vessel embolism and tyloses in early stages of Pierce's disease. *Australian Journal of Grape and Wine Research* **22**: 81–86.

Pouzoulet J, **Pivovaroff AL**, **Santiago LS**, **Rolshausen PE. 2014**. Can vessel dimension explain tolerance toward fungal vascular wilt diseases in woody plants? Lessons from Dutch elm disease and esca disease in grapevine. *Frontiers in Plant Science* **5**: 1–11.

Pouzoulet J, **Scudiero E**, **Schiavon M**, **Rolshausen PE. 2017**. Xylem vessel diameter affects the compartmentalization of the vascular pathogen *Phaeomoniella chlamydospora* in grapevine. *Frontiers in Plant Science* **8**: 1–13.

Prats KA, **Fanton AC**, **Brodersen CR**, **Furze ME. 2023**. Starch depletion in the xylem and phloem ray parenchyma of grapevine stems under drought. *AoB Plants* **15**: 1–12.

Redak RA, **Purcell AH**, **Lopes JRS**, **Blua MJ**, **Mizell RF III**, **Andersen PC. 2004**. The biology of xylem fluid–feeding insect vectors of *Xylella fastidiosa* and their relation to disease epidemiology. *Annual Review of Entomology* **49**: 243–270.

Riaz S, **Tenscher AC**, **Rubin J**, **Graziani R**, **Pao SS**, **Walker MA. 2008**. Fine-scale genetic mapping of two Pierce's disease resistance loci and a major segregation distortion region on chromosome 14 of grape. *TAG. Theoretical and Applied Genetics. Theoretische und angewandte Genetik* **117**: 671–681.

Riaz S, **Tenscher AC**, **Heinitz CC**, **Huerta-Acosta KG**, **Walker MA. 2020**. Genetic analysis reveals an east-west divide within North American *Vitis* species that mirrors their resistance to Pierce's disease. *PLoS One* **15**: e0243445.

Roper MC, **Greve LC**, **Warren JG**, **Labavitch JM**, **Kirkpatrick BC. 2007**. *Xylella fastidiosa* requires polygalacturonase for colonization and pathogenicity in *Vitis vinifera* grapevines. *Molecular Plant-Microbe Interactions* **20**: 411–419.

Roper C, **Castro C**, **Ingel B. 2019**. *Xylella fastidiosa*: bacterial parasitism with hallmarks of commensalism. *Current Opinion in Plant Biology* **50**: 140–147.

Schubert A, **Lovisolo C**, **Peterlunger E. 1999**. Shoot orientation affects vessel size, shoot hydraulic conductivity and shoot growth rate in *Vitis vinifera* L. *Plant, Cell & Environment* **22**: 197–204.

Shigo AL. 1985. Compartmentalization of decay in trees. *Scientific American* **252**: 96–103.

Shtein I, **Hayat Y**, **Munitz S**, ***et al***. **2017**. From structural constraints to hydraulic function in three *Vitis* rootstocks. *Trees* **31**: 851–861.

Sun Q, **Greve LC**, **Labavitch JM. 2011**. Polysaccharide compositions of intervessel pit membranes contribute to Pierce's disease resistance of grapevines. *Plant Physiology* **155**: 1976–1987.

Sun Q, **Sun Y**, **Walker MA**, **Labavitch JM. 2013**. Vascular occlusions in grapevines with Pierce's disease make disease symptom development worse. *Plant Physiology* **161**: 1529–1541.

Sun Q, **Sun Y**, **Juzenas K. 2017**. Immunogold scanning electron microscopy can reveal the polysaccharide architecture of xylem cell walls. *Journal of Experimental Botany* **68**: 2231–2244.

Thorne ET, **Stevenson JF**, **Rost TL**, **Labavitch JM**, **Matthews MA. 2006**. Pierce's disease symptoms: comparison with symptoms of water deficit and the impact of water deficits. *American Journal of Enology and Viticulture* **57**: 11.

Tyree MT, **Zimmermann MH. 2002**. *Xylem structure and the ascent of sap.* Berlin: Springer.

Varela LG, **Smith RJ**, **Phillips PA. 2001**. *Pierce's disease.* Oakland, CA: University of California, Division of Agricultural and Natural Resources.

Walker NC, **Ruiz SA**, **Ferreira TR**, ***et al***. **2023***a*. A high-throughput analysis of high-resolution X-ray CT images of stems of olive and citrus plants resistant and susceptible to *Xylella fastidiosa*. *Plant Pathology* **00**: 1–14.

Walker NC, **White SM**, **McKay Fletcher D**, ***et al***. **2023***b*. The impact of xylem geometry on olive cultivar resistance to *Xylella fastidiosa*: an image-based study. *Plant Pathology* **72**: 521–535.

Wason J, **Bouda M**, **Lee EF**, ***et al***. **2021**. Xylem network connectivity and embolism spread in grapevine (*Vitis vinifera* L.). *Plant Physiology* **186**: 373–387.

Wells JM, **Raju BC**, **Hung H-Y**, **Weisburg WG**, **Mandelco-Paul L**, **Brenner DJ. 1987**. *Xylella fastidiosa* gen. nov., sp. nov: gram-negative, xylem-limited, fastidious plant bacteria related to *Xanthomonas* spp. *International Journal of Systematic Bacteriology* **37**: 136–143.

Yadeta KA, **Thomma BPHJ. 2013**. The xylem as battleground for plant hosts and vascular wilt pathogens. *Frontiers in Plant Science* **4**: 1–12.

Zaini PA, **Nascimento R**, **Gouran H**, ***et al***. **2018**. Molecular profiling of Pierce's disease outlines the response circuitry of *Vitis vinifera* to *Xylella fastidiosa* infection. *Frontiers in Plant Science* **9**: 771.